Liquid-Crystal Active Tamm-Plasmon Devices

Hao-Chi Cheng,[1] Ching-Yung Kuo,[2] Yu-Ju Hung,[2] Kuo-Ping Chen,[1] and Shie-Chang Jeng[1,*]
[1]*Institute of Imaging and Biomedical Photonics, National Chiao Tung University, Tainan 711, Taiwan*
[2]*Department of Photonics, National Sun Yat-sen University, Kaohsiung 804, Taiwan*

(Received 17 October 2017; revised manuscript received 17 December 2017; published 20 June 2018)

We demonstrate a liquid-crystal (LC)-tuned Tamm-plasmon (TP) resonance device. The term TP polariton refers to plasmonic resonance at the interface between a photonic crystal (PC) and a metallic film. We formulate a precise optical analysis of the proposed device using the transfer-matrix method. A single resonance dip in the photonic band-gap region guarantees that the thickness of the LC layer between the PC and the metallic film can be as small as about 180 nm. Tuning phase retardation in the LC layer is shown to shift the resonance wavelength tens of nanometers, depending on the birefringence and width of the LC layer. Simulation results are in good agreement with the experimental data.

DOI: 10.1103/PhysRevApplied.9.064034

I. INTRODUCTION

Surface states were first described by the Russian scientist Igor E. Tamm, who received a Nobel Prize for his efforts in 1958 [1–3]. The behavior of electrons in a periodic crystal follows the band diagrams derived from the arrangement of atoms. When the periodic structure is terminated at a particular point, the surface states are the eigenstates lying in the band-gap region. The propagation wave vector perpendicular to the surface of the crystal becomes imaginary; however, it is real along the surface. The Tamm-plasmon (TP) mode is a surface mode that occurs at the interface between a metallic film and the photonic-crystal (PC) substrate [4–6]. The resonance wavelength of a TP device depends on the central wavelength of the PC, the characteristics of the metallic film, and the thickness and refractive index of the top layer of the PC [7–11]. It is interesting to note that this mode lies partially within the light cone when the in-plane k vector is near zero and the medium of the light cone is air, which means that it can be excited without an additional phase-matching component [4–14]. Vertical illumination causes it to be excited only if the wavelength matches the design of the periodic structure. Detailed discussions on the dispersion characteristics in this mode are included in Refs. [12–14]. Bloch surface waves and the TP mode are both surface modes on a PC substrate, formed, respectively, by an abnormal dielectric or a metallic film capping a PC substrate. The difference lies in the fact that the skin depth of a noble metal in the visible wavelength range is in the tens of nanometers, whereas in a dielectric top layer, the skin depth is in the hundreds of nanometers. Researchers have demonstrated interactions between TP modes and surface-plasmon modes or cavity modes [15,16], and TP devices have been applied in lasers, sensors, and filters [17–22]. However, actively tuning the TP mode beneath the top metallic film is difficult. Because of the strong localization of electric fields between metals and PC at the resonance wavelength of the TP device, perturbations above the metallic film have only tiny effects. The fact that the resonance wavelength cannot be altered after the TP device has been fabricated greatly limits the applicability of these devices. Tunable TP devices have been demonstrated only in semiconductor laser systems, which involve heating or carrier injection during lasing [23,24].

Numerous tunable photonic devices have been developed using liquid crystals (LCs) due to their large birefringence and controllability via external (electrical, optical, or thermal) stimuli [25–28]. Tunable surface-plasmon-polariton (SPP) or localized surface-plasmon resonance with LCs have also been widely demonstrated in previous works [29–36], in the development of tunable plasmonic color filters [25,31], metasurfaces [33,35], and devices with a fast tuning response [34]. However, LCs have seldom been used to tune TP resonance due to the difficulties associated with inserting a thin layer of LCs between the metal and the PC. Furthermore, surface anchoring effects restrict the efficiency of optical tuning in most LC-plasmon hybrid devices [35–39]. In the proposed TP scheme, the phase retardation of the LC layer is an ensemble effect from the entire layer, rather than the effect of individual molecules adjacent to the metal surface. The difference in our method lies in the creation of a small LC gap layer (<200 nm) between the metal and the PC, which gives the LC space in which to change its orientation. Unlike most existing SPP devices fabricated using e-beam lithography, our scheme is highly amenable to

*To whom all correspondence should be addressed.
scjeng@faculty.nctu.edu.tw

 © 2018 American Physical Society

scaling up for practical applications. Fabrication of the PC substrate is achieved using mature thin-film processes, which can be scaled up to several meters. We also use temperature-based tuning as the modulation method. In simulations, the transfer-matrix method is used to examine the resonance effects on tunable TP devices, the results of which are in good agreement with experiment results.

II. THEORETICAL MODELING

Figure 1(a) presents the coordinates of the proposed system, and Fig. 1(b) illustrates the layered structure. The LC layer is sandwiched between a PC substrate and Au-coated glass. The one-dimensional PC substrate lies along the x-y plane. (θ, ϕ) is defined according to director $\mathbf{n}$ of the liquid crystal, as shown in Fig. 1(a). The LC molecules are homogeneously aligned within the TP device. The refractive index is described using Eqs. (1) and (2), where (k_x, k_y, and k_z) are the k vectors of the incident light in the corresponding layer, and n_e and n_o are the ellipsoidal refractive indices of the LC molecules. For ellipsoid and spherical equations,

$$\frac{(k_x\cos\theta + k_y\sin\theta)^2}{{n_o}^2{k_0}^2} + \frac{{k_y}^2}{{n_e}^2{k_0}^2} + \frac{(-k_x\sin\theta + k_{ze}\cos\theta)^2}{{n_e}^2{k_0}^2} = 1, \tag{1}$$

$$\frac{{k_x}^2}{{k_0}^2} + \frac{{k_y}^2}{{k_0}^2} + \frac{{k_{zo}}^2}{{k_0}^2} = {n_o}^2. \tag{2}$$

According to previous reports [39,40], the two eigen E-fields, E_o and E_e, in the liquid-crystal layer can be expressed as follows:

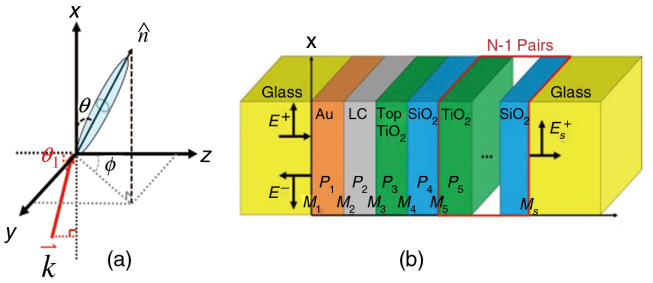

FIG. 1. (a) Coordinates of LC molecules and the proposed system. (b) LC layer sandwiched between the PC substrate and Au-covered glass.

E_o:

$$\begin{bmatrix} E_{2xo} \\ E_{2yo} \\ E_{2zo} \end{bmatrix} = \begin{bmatrix} \sin\phi\cos\theta k_{2zo} \\ \sin\theta k_x - \cos\theta\cos\phi k_{2zo} \\ -\sin\phi\cos\theta k_x \end{bmatrix}, \tag{3}$$

E_e:

$$\begin{bmatrix} E_{2xe} \\ E_{2ye} \\ E_{2ze} \end{bmatrix} = \begin{bmatrix} -\cos\theta\cos\phi{k_{zo}}^2 + \sin\theta k_x k_{2ze} \\ -{n_o}^2\cos\theta\sin\phi{k_0}^2 \\ \cos\theta\cos\phi k_x k_{2ze} + \sin\theta({k_{2ze}}^2 - {n_o}^2{k_0}^2) \end{bmatrix}, \tag{4}$$

where

$$k_x = k_{1x} = k_{2x} = n_1 k_0 \sin\theta_1, \tag{5}$$

$$k_{2zo} = \sqrt{{n_o}^2{k_0}^2 - {k_x}^2}, \tag{6}$$

$$k_{2ze} = \frac{({n_o}^2 - {n_e}^2)\cos\theta\sin\theta\cos\phi k_x + \sqrt{{n_o}^2{n_e}^2({n_e}^2\sin^2\theta + {n_o}^2\cos^2\theta){k_0}^2 - [{n_o}^2{n_e}^2(\sin^2\theta\sin^2\phi + \cos^2\phi) + {n_o}^4\cos^2\theta\sin^2\phi]{k_x}^2}}{{n_e}^2\sin^2\theta + {n_o}^2\cos^2\theta}, \tag{7}$$

where Eqs. (6) and (7) are derived from Eqs. (1) and (2). θ_1 is the incidence angle.

The transfer-matrix method requires that the reflection and transmission coefficients be derived precisely at each interface. In an isotropic medium, the transverse magnetic (TM) and transverse electric (TE) modes are in the corresponding eigenstates; however, this is not the case when dealing with a birefringent layer. Reflections from and transmission through this birefringent layer can result in coupling between the TE and TM modes. The complex analysis involved in this interaction will be described in another report. In this paper, we describe only the simplest case, where (θ, ϕ) is set to (0°–90°, 90°), such that the LC lies along the x-y plane and rotates around the z axis. In this scenario, the TM field is incident to the LC layer with the k vector defined as $(k\sin\theta_1,\ 0\ ,\ k\cos\theta_1)$, as shown in Fig. 1(a). The director of the LC is rotated around the z axis, wherein only e-light in the LC is excited, resulting in a clear interfacial matrix.

Figure 2 presents a detailed analysis of the associated fields. Mediums 1 and 3 are isotropic layers, whereas medium 2 is a LC layer. The TM field is incidental to medium 1, and the continuity and boundary conditions of E_x and H_y produce the following coefficients [41,42]:

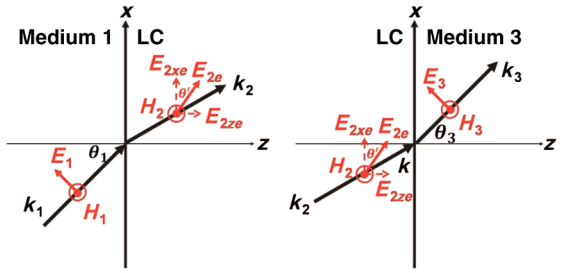

FIG. 2. Detailed description of fields at interfaces adjacent to the LC layer.

$$r_{12} = \frac{n_1 k_0 - \cos\theta_1 (k_{2z} - k_x \tan\theta')}{n_1 k_0 + \cos\theta_1 (k_{2z} - k_x \tan\theta')}, \tag{8}$$

$$t_{12} = \frac{2 n_1 k_0 \cos\theta_1}{(n_1 k_0 + k_{2z}\cos\theta_1)\cos\theta' - k_x \cos\theta_1 \sin\theta'}, \tag{9}$$

$$r_{23} = \frac{k_{2z}\cos\theta'\cos\theta_3 - k_x \sin\theta'\cos\theta_3 - n_3 k_0 \cos\theta'}{k_{2z}\cos\theta'\cos\theta_3 - k_x \sin\theta'\cos\theta_3 + n_3 k_0 \cos\theta'}, \tag{10}$$

$$t_{23} = \frac{2(k_{2z}\cos\theta'\cos\theta' - k_x \cos\theta'\sin\theta')}{k_{2z}\cos\theta'\cos\theta_3 - k_x \sin\theta'\cos\theta_3 + n_3 k_0 \cos\theta'} \tag{11}$$

$$\theta' = \tan^{-1}\frac{E_{2ze}}{E_{2xe}}. \tag{12}$$

The subscript 12 refers to light traveling from layer 1 to layer 2. The interfacial matrix M is composed as follows:

$$M = \begin{bmatrix} \frac{1}{t} & \frac{r}{t} \\ \frac{1}{t} & \frac{r}{t} \end{bmatrix}, \tag{13}$$

and the propagation matrix P is composed as follows:

$$P = \begin{bmatrix} e^{jk_z d} & 0 \\ 0 & e^{-jk_z d} \end{bmatrix}. \tag{14}$$

The stacked layered matrix can be expressed in terms of the scheme in Fig. 1(b) as follows:

$$\begin{bmatrix} E^+ \\ E^- \end{bmatrix} = M_1 P_1 M_2 P_2 M_3 P_3 M_4 \times P_4 (M_5 P_5 M_4 P_4)^{N-1} M_s \begin{bmatrix} E_S{}^+ \\ 0 \end{bmatrix}. \tag{15}$$

III. EXPERIMENTAL PROCEDURES

The TP device in Fig. 1(b) is designed using a standard quarter-wavelength PC with a central wavelength λ_0 of approximately 680 nm. The PC comprises eight paired layers of TiO_2 and SiO_2 deposited on a B270 glass substrate using electron-beam evaporation with ion-beam-assisted deposition (Kingmate Electronics) to depths of 78 and 119 nm, respectively. The thickness of the TiO_2 top layer is about 205 nm. This layer undergoes buffing with a nylon cloth to achieve a homogeneous alignment of LC molecules. A thin gold film is applied to a depth of approximately 30 nm on a glass substrate using a thermal evaporator. The Au-coated substrate and the PC are then assembled with a small gap between them to form a tunable TP device. In each run of the experiment, the width of the gap is varied, with the aim of optimizing the measured resonance wavelengths. The gap is then filled with LC molecules (5CB, $n_e \sim 1.68$, $n_o \sim 1.53$ at $T \sim 30\,^\circ\mathrm{C}$, $n_{\mathrm{iso}} \sim 1.58$, $T_c \sim 35\,^\circ\mathrm{C}$). As the LC is filled, the cell is heated to about 36 °C (above the clearing point) to obtain uniform alignment. The resonance wavelength of the TP device is tuned by changing the phase of the 5CB LC between the nematic phase and the isotropic phase. It is realized by changing the temperature of 5CB LC via a thermoelectric device attached to the bottom of the TP device. When the driving voltage of the thermoelectric device is 0.4 or 0.5 V, therefore, the TP device is held at approximately 30 °C and about 36 °C, respectively. This voltage control of the thermoelectric device makes it possible to switch the LC layer in the TP device between the nematic phase (approximately 30 °C) and the isotropic phase (about 36 °C) while operating the thermoelectric device at 0.4 and 0.5 V, respectively.

Figure 3 presents the apparatus used to measure the reflectance spectra of the tunable TP device. It is set up by a spectrometer (Ocean Optics HR4000) via a polarizing optical microscope (Olympus BX51). A white light illuminates the TP device from the metal side. An aluminum mirror (Thorlabs, ME1-G01) is applied for the reflectance reference. The polarization of input light through the upright optical microscope lies along the x axis, and the

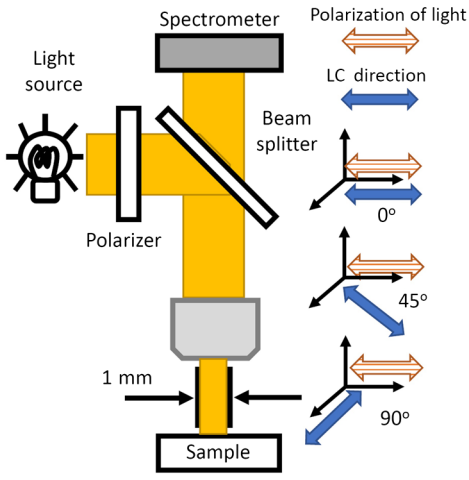

FIG. 3. Measurement system for reflectance spectra of the TP devices.

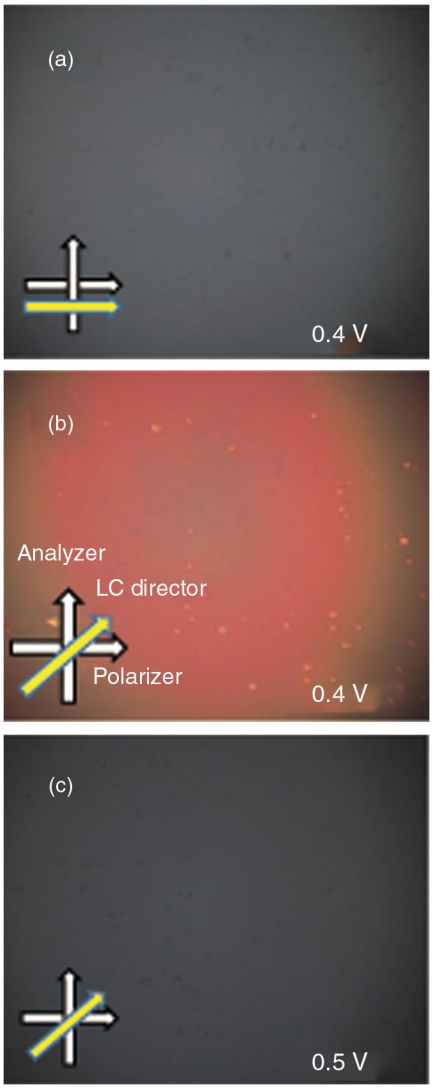

FIG. 4. Photographic images of the TP devices under a polarized light microscope, where the LC layer is in (a) the nematic phase, (b) the nematic phase, and (c) the isotropic phase.

surface of the sample is along the x-y plane. The direction of the LC director (defined as θ) is rotated to 0°, 45°, and 90° on the x-y plane. The birefringence of the LC layer makes the resulting TP device polarization dependent. Figure 4 presents images of the tunable TP device obtained under a polarized light microscope. Figures 4(a) and 4(b) show the homogeneous alignment of the LC molecules within the TP device. As shown in Figs. 4(b) and 4(c), the LC layer is in nematic and isotropic phases when the thermoelectric device is operated at 0.4 and 0.5 V, respectively.

IV. EXPERIMENTAL RESULTS AND DISCUSSION

Figure 5 presents the reflectance spectra of the TP device before and after filling the LCs, i.e., with the LC layer in an isotropic phase. After LC filling, the resonance wavelength

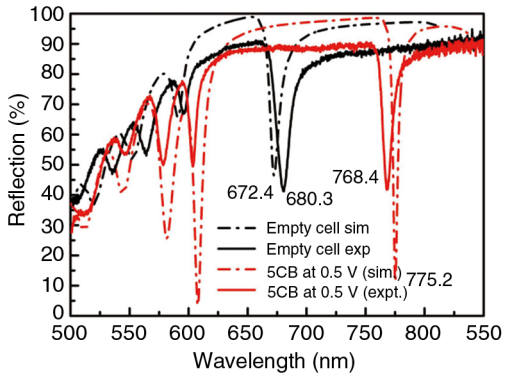

FIG. 5. Reflectance spectra of the TP devices before and after LC filling, wherein the LC layer is in the isotropic phase.

shifts from 680.3 to 768.4 nm due to a difference in refractive index from 1 (air) to 1.58 (LC_{iso}). In simulations, the cell gap is estimated at about 317 nm. The dotted curves indicate the simulation results. Discrepancies between the simulation results and the experimental data can be attributed to imperfections in the PC substrate, the gold film, or the gap nonuniformity [7–9].

Figure 6 presents polarization-dependent measurements of the TP device, where the LC layer is operated in nematic phase and the cell gap is set at approximately 180 nm. The resonance wavelengths are 651.4 and 667.6 nm when the θ values are 90° and 0°, respectively. The corresponding refractive indices of the incident lights are n_o and n_e, respectively. Based on Eq. (15) and the cell structure adopted in Fig. 6, the reflection spectrum with respect to the LC angle θ is shown in Fig. 7. TP resonance can be tuned from 668 to 651 nm simply by rotating the LC molecules from 0° to 90° with a reflection resonance dip of only about 45% in the band-gap region under normal incidence. The low coupling ratio is due to several factors, such as the quality of metallic film and the film thickness [7–9]. A higher coupling ratio in the TP can also be achieved when the incidence is tilted and the TPs have an in-plane propagation k vector. Figure 8 presents the

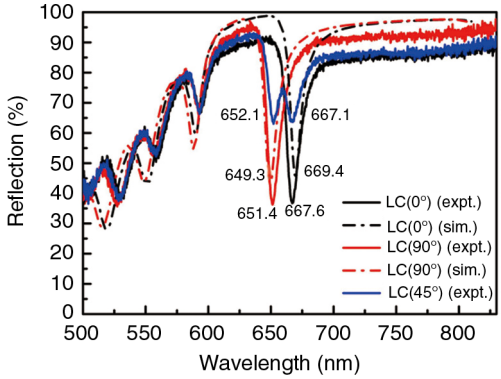

FIG. 6. Reflectance spectra of the TP devices measured at three angles θ, where the LC layer is in the nematic phase.

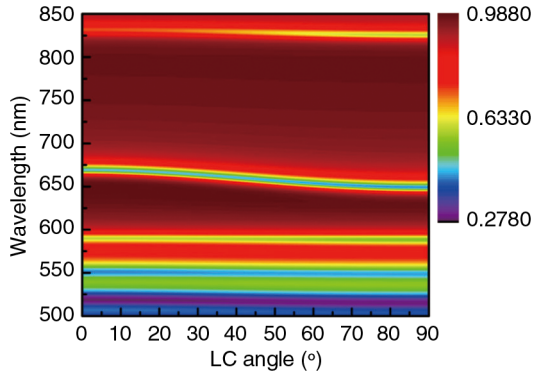

FIG. 7. Reflectance spectrum vs LC rotation.

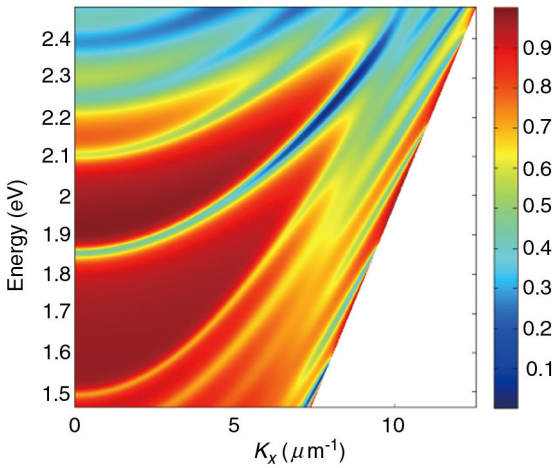

FIG. 8. Reflection spectrum vs in-plane k vector.

reflection spectrum with respect to the parallel k vector. With an increase in the in-plane k vector, the resonance dip presents stronger (blue) coupling in the TP mode.

Figure 9 presents the measured tuning spectrum of the TP device under two LC phases (with a LC width of approximately 180 nm). The resonance dips based on different polarization incidences are evaluated. The two resonance wavelengths (667.1 and 652.1 nm at $\theta = 45°$) present homogeneous alignment. As expected, the resonance wavelengths at $\theta = 45°$ are a combination of resonance wavelengths at $\theta = 0°$ and $\theta = 90°$. The red curves are measured by heating the device to an isotropic state, which is polarization independent. The active tuning range depends on the direction of incident light polarization, the direction of LC alignment, and the LC gap. Figure 10 illustrates the dependence of resonance wavelengths on the width of the LC gap, where the LC layer is operated in the nematic ($\theta = 0°$) and isotropic phases. An increase in the gap is shown to increase the tuning range. The accumulated difference in optical path between the two LC orientation states increases the tuning range until the gap reaches 700 nm, at which point a second resonance dip appears in the photonic band-gap region, thereby

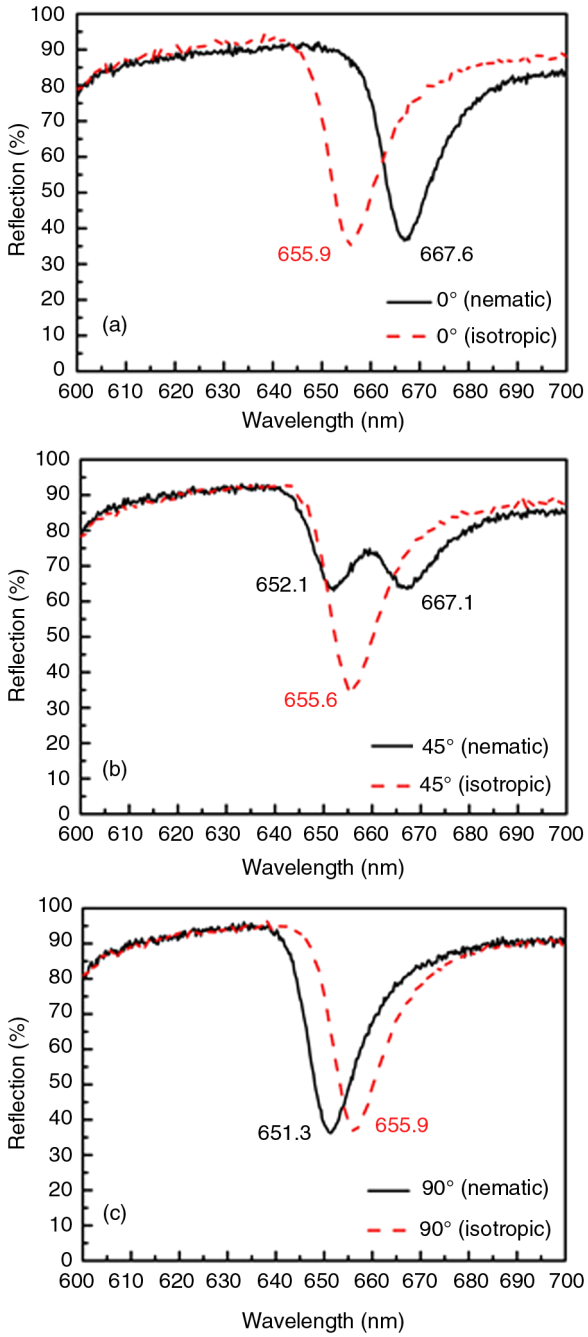

FIG. 9. Reflectance spectra of TP devices with a LC layer switched between the nematic and isotropic phases, measured at (a) $\theta = 0°$, (b) $\theta = 45°$, and (c) $\theta = 90°$.

complicating the situation. The periodic behavior of the resonance wavelength is due to the cycling of resonance dips in the photonic band-gap region.

It should be noted that the resonance wavelength can be tuned by changing the phase of the LC or by changing the LC gap. We recently developed a scheme by which to tune the resonance wavelength by changing the LC gap using fine screws and piezoelectric (PZT) tubes, as shown in Fig. 11. The resonance wavelength of a TP device is

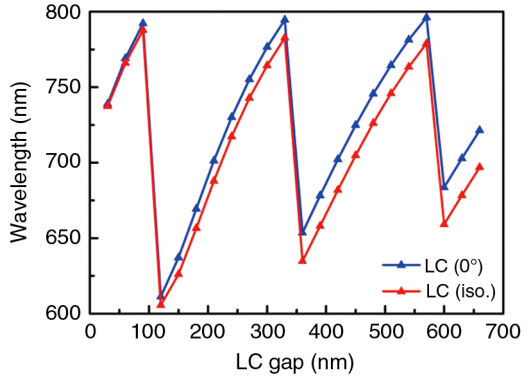

FIG. 10. Relationship between the resonance wavelength of the Tamm-plasmon mode and the LC gap width, where the LC layer is operated at the nematic state ($\theta = 0°$) and the isotropic state.

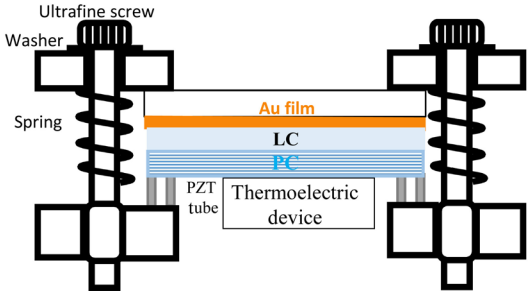

FIG. 11. An apparatus for changing the LC gap by using fine screws and PZT tubes.

generally fixed during device fabrication. The LC gap can be adjusted manually to a value corresponding to a specific resonance wavelength using fine screws, the preliminary results of which are presented in Fig. 12. The figure shows two resonance wavelengths related to two different LC gaps. It would also be possible to control the LC gap by applying voltage to PZT tubes. For a PZT tube with a length L, the change in length ΔL can be determined using the equation below [43]:

$$\Delta L = (d_{31} V L)/t, \tag{16}$$

where d_{31} is the piezoelectric constant, V is the voltage applied to the PZT tube, and L and t are the length and the wall thickness of a PZT tube, respectively. Thus, if $d_{31} = 0.1$ nm/V, $L = 10$ mm, and $t = 1$ mm, then an applied voltage of 200 V would alter the LC gap by about 200 nm. This change of LC gap, in turn, would produce a resonance shift of up to 200 nm, depending on the initial LC gap estimated in Fig. 10. This would be a remarkable amount of variation in an optical filter or switch application. Changing the LC phase in conjunction with electrical control over the LC gap allows for a tuning of the resonance wavelength over a wide range. Experiments on the TP device using PZT tubes are currently in progress.

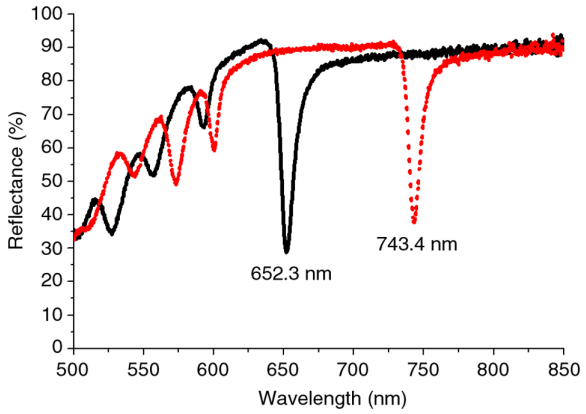

FIG. 12. Reflectance spectra of the TP devices at two different LC gaps, wherein the LC layer is in the isotropic phase.

V. CONCLUSIONS

In conclusion, a tunable Tamm-plasmon device is demonstrated in this paper by filling LC molecules in the subwavelength gap between the metallic film and the PC. The resonance wavelength of the TP device is switched by changing the temperature of the LC layer. Depending on the angles between the directions of the incident light polarization and the LC director, the resonance wavelength shows a shift of approximately 4–11 nm when the LC layer (LC width, about 180 nm) is changed from the nematic to the isotropic phase. A shift of 15.5 nm can also be obtained for a LC director rotating 90° on the substrate surface. This tuning effect could be applied to the switching of optical planar circuits and quantum-dot laser emission.

ACKNOWLEDGMENTS

The authors would like to thank the Ministry of Science and Technology of Taiwan for financially supporting this research under Contracts No. MOST 103-2112-M-009-013-MY3, No. MOST 106-2112-M-009-003, No. MOST 105-2221-E-009-096-MY2, and No. MOST 105-2112-M-110-008. We also thank the anonymous reviewers for their constructive comments.

[1] I. E. Tamm, On the possible bound states of electrons on a crystal surface, Z. Phys. Sowjetunion **1**, 733 (1932).
[2] W. Shockley, On the surface states associated with a periodic potential, Phys. Rev. **56**, 317 (1939).
[3] S. G. Davison and M. Stęślicka, *Basic Theory of Surface States* (Oxford University Press, Oxford, 1992).
[4] M. Kaliteevski, I. Iorsh, S. Brand, R. A. Abram, J. M. Chamberlain, A. V. Kavokin, and I. A. Shelykh, Tamm plasmon-polaritons: Possible electromagnetic states at the interface of a metal and a dielectric Bragg mirror, Phys. Rev. B **76**, 165415 (2007).
[5] M. E. Sasin, R. P. Seisyan, M. A. Kaliteevski, S. Brand, R. A. Abram, J. M. Chamberlain, I. V. Iorsh, I. A. Shelykh,

A. Yu. Egorov, A. P. Vasil'ev, V. S. Mikhrin, and A. V. Kavokin, Tamm plasmon-polaritons: First experimental observation, Superlattices Microstruct. **47**, 44 (2010).

[6] K. Leosson, S. Shayestehaminzadeh, T. K. Tryggvason, A. Kossoy, B. Agnarsson, F. Magnus, S. Olafsson, J. T. Gudmundsson, E. B. Magnusson, and I. A. Shelykh, Comparing resonant photon tunneling via cavity modes and Tamm plasmon polariton modes in metal-coated Bragg mirrors, Opt. Lett. **37**, 4026 (2012).

[7] O. Gazzano, S. M. de Vasconcellos, K. Gauthron, C. Symonds, J. Bloch, P. Voisin, J. Bellessa, A. Lemaître, and P. Senellart, Evidence for Confined Tamm Plasmon Modes under Metallic Microdisks and Application to the Control of Spontaneous Optical Emission, Phys. Rev. Lett. **107**, 247402 (2011).

[8] H. Zhou, G. Yang, K. Wang, H. Long, and P. Lu, Multiple optical Tamm states at a metal-dielectric mirror interface, Opt. Lett. **35**, 4112 (2010).

[9] C. Y. Chang, Y. H. Chen, Y. L. Tsai, H. C. Kuo, and K. P. Chen, Tunability and optimization of coupling efficiency in Tamm plasmon modes, IEEE J. Sel. Top. Quantum Electron. **21**, 262 (2015).

[10] G. Isic, S. Vukovic, Z. Jasic, and M. Belic, Tamm plasmon modes on semi-infinite metallodielectric superlattices, Sci. Rep. **7**, 3746 (2017).

[11] S. Azzini, G. Lheureux, C. Symonds, J.-M. Benoit, P. Senellart, A. Lemaitre, J.-J. Greffet, C. Blanchard, C. Sauvan, and J. Bellessa, Generation and spatial control of hybrid Tamm plasmon/surface plasmon modes, ACS Photonics **3**, 1776 (2016).

[12] C. Liu, M. Kong, and B. Li, Tamm plasmon-polariton with negative group velocity induced by a negative index metamaterial capping layer at metal-Bragg reflector interface, Opt. Express **22**, 11376 (2014).

[13] S. Brand, M. A. Kaliteevski, and R. A. Abram, Optical Tamm states above the bulk plasma frequency at a Bragg stack/metal interface, Phys. Rev. B **79**, 085416 (2009).

[14] G. Isić, S. Vuković, Z. Jašić, and M. Belić, Tamm plasmon modes on semi-infinite metallodielectric superlattices, Sci. Rep. **7**, 3746 (2017).

[15] B. I. Afinogenov, V. O. Bessonov, A. A. Nikulin, and A. A. Fedyanin, Observation of hybrid state of Tamm and surface plasmon-polaritons in one-dimensional photonic crystals, Appl. Phys. Lett. **103**, 061112 (2013).

[16] S. Rahman, T. Klein, S. Klembt, J. Gutowski, D. Hommel, and K. Sebald, Observation of a hybrid state of Tamm plasmons and microcavity exciton polaritons, Sci. Rep. **6**, 34392 (2016).

[17] W. L. Zhang, F. Wang, Y. J. Rao, and Y. Jiang, Novel sensing concept based on optical Tamm plasmon, Opt. Express **22**, 14524 (2014).

[18] X. Luo, X. Zhai, L. Wang, Q. Lin, and J. Liu, Tunable terahertz narrow-band plasmonic filter based on optical Tamm plasmon in dual-section InSb slot waveguide, Plasmonics **12**, 509 (2017).

[19] C. Symonds, A. Lemaitre, P. Senellart, M. H. Jomaa, S. A. Guebrou, E. Homeyer, G. Brucoli, and J. Bellessa, Lasing in a hybrid GaAs/silver Tamm structure, Appl. Phys. Lett. **100**, 121122 (2012).

[20] S. Kumar, P. S. Maji, and R. Das, Tamm-plasmon resonance based temperature sensor in a Ta_2O_5/SiO_2 based distributed Bragg reflector, Sens. Actuators A **260**, 10 (2017).

[21] S.-G. Huang, K.-P. Chen, and S.-C. Jeng, Phase sensitive sensor on Tamm plasmon devices, Opt. Mater. Express **7**, 1267 (2017).

[22] C. Symonds, G. Lheureux, J. P. Hugonin, J. J. Greffet, J. Laverdant, G. Brucoli, A. Lemaitre, P. Senellart, and J. Bellessa, Confined Tamm plasmon lasers, Nano Lett. **13**, 3179 (2013).

[23] J. Gessler, V. Baumann, M. Emmerling, M. Amthor, K. Winkler, S. Höfling, C. Schneider, and M. Kamp, Electro optical tuning of Tamm-plasmon exciton-polaritons, Appl. Phys. Lett. **105**, 181107 (2014).

[24] C. Grossmann, C. Coulson, G. Christmann, I. Farrer, H. Beere, D. Ritchie, and J. Baumberg, Tuneable polaritonics at room temperature with strongly coupled Tamm plasmon polaritons in metal/air-gap microcavities, Appl. Phys. Lett. **98**, 231105 (2011).

[25] D. Franklin, Y. Chen, A. Vazquez-Guardado, S. Modak, J. Boroumand, D. M. Xu, S. T. Wu, and D. Chanda, Polarization-independent actively tunable colour generation on imprinted plasmonic surfaces, Nat. Commun. **6**, 7337 (2015).

[26] I. Abdulhalim, Liquid crystal active nanophotonics and plasmonics: From science to devices, J. Nanophoton. **6**, 061001 (2012).

[27] J. Olson, A. Manjavacas, T. Basu, D. Huang, A. E. Schlather, B. Zheng, N. J. Halas, P. Nordlander, and S. Link, High chromaticity aluminum plasmonic pixels for active liquid crystal displays, ACS Nano **10**, 1108 (2016).

[28] Y. J. Liu, Y. B. Zheng, J. Liou, I.-K. Chiang, I. C. Khoo, and T. J. Huang, All-optical modulation of localized surface plasmon coupling in a hybrid system composed of photoswitchable gratings and Au nanodisk arrays, J. Phys. Chem. C **115**, 7717 (2011).

[29] R. Luo, Y. Gu, X. K. Li, L. J. Wang, I. C. Khoo, and Q. H. Gong, Mode recombination and alternation of surface plasmons in anisotropic mediums, Appl. Phys. Lett. **102**, 011117 (2013).

[30] X. L. Wang, P. Wang, J. X. Chen, Y. H. Lu, H. Ming, and Q. W. Zhan, Theoretical and experimental studies of surface plasmons excited at metal-uniaxial dielectric interface, Appl. Phys. Lett. **98**, 021113 (2011).

[31] Z.-W. Xie, J.-H. Yang, V. Vashistha, W. Lee, and K.-P. Chen, Liquid-crystal tunable color filters based on aluminum metasurfaces, Opt. Express **25**, 30764 (2017).

[32] X. Wang, D.-H. Kwon, D. H. Werner, I.-C. Khoo, A. V. Kildishev, and V. M. Shalaev, Tunable optical negative-index metamaterials employing anisotropic liquid crystals, Appl. Phys. Lett. **91**, 143122 (2007).

[33] J. Sautter, I. Staude, M. Decker, E. Rusak, D. N. Neshev, I. Brener, and Y. S. Kivshar, Active tuning of all-dielectric metasurfaces, ACS Nano **9**, 4308 (2015).

[34] M. V. Gorkunov, I. V. Kasyanova, V. V. Artemov, M. I. Barnik, A. R. Geivandov, and S. P. Palto, Fast Surface-Plasmon-Mediated Electro-Optics of a Liquid Crystal on a Metal Grating, Phys. Rev. Applied **8**, 054051 (2017).

[35] O. Buchnev, N. Podoliak, M. Kaczmarek, N. I. Zheludev, and V. A. Fedotov, Electrically controlled nanostructured

metasurface loaded with liquid crystal: Toward multifunctional photonic switch, Adv. Opt. Mater. **3**, 674 (2015).
[36] P. A. Kossyrev, A. J. Yin, S. G. Cloutier, D. A. Cardimona, D. H. Huang, P. M. Alsing, and J. M. Xu, Electric field tuning of plasmonic response of nanodot array in liquid crystal matrix, Nano Lett. **5**, 1978 (2005).
[37] M. Decker, Ch. Kremers, A. Minovich, I. Staude, A. E. Miroshnichenko, D. Chigrin, D. N. Neshev, Ch. Jagadish, and Yu. S. Kivshar, Electro-optical switching by liquid-crystal controlled metasurfaces, Opt. Express **21**, 8879 (2013).
[38] I. C. Khoo, Nonlinear optics, active plasmonics and metamaterials with liquid crystals, Prog. Quantum Electron. **38**, 77 (2014).
[39] Y. R. Yen, T. H. Lee, Z. Y. Wu, T. H. Lin, and Y. J. Hung, Comprehensive three-dimensional analysis of surface plasmon polariton modes at uniaxial liquid crystal-metal interface, Opt. Express **23**, 32377 (2015).
[40] Y. J. Hung, Y. R. Yen, and I. S. Lin, Fresnel analysis of Kretschmann geometry with a uniaxial crystal layer on a three-layered film, AIP Adv. **6**, 045023 (2016).
[41] S. J. Orfanidis, *Electromagnetic Waves and Antennas* (Rutgers University, New Brunswick, 2002).
[42] B. Guenther, *Modern Optics* (Oxford University Press, Oxford, 2015).
[43] Boston Piezo-Optics, Inc., http://www.bostonpiezooptics.com (8 March 2018).